SciEn

*Proceedings of 8th International Conference on Mechanical, Industrial and Energy Engineering 2024*
*02-04 January, 2025, Khulna, BANGLADESH*

SciEn Conference Series: Engineering Vol. 3, 2025, pp 707-712 https://doi.org/10.38032/scse.2025.3.180

# Numerical Investigation on the Effect of Converging Channel in Crossflow Heat Exchanger

*Adnan Roshid Shawon*, Fahim Al Galib, Mohammad Ilias Inam*

Department of Mechanical Engineering, Khulna University of Engineering & Technology, Khulna-9203, Bangladesh

**ABSTRACT**

The objective of this numerical study is to investigate the effect of converging channel in crossflow heat exchanger using Rectangular Winglet Pair (RWP) in different arrangement from the tube center. For a defined converging angle, the placement of RWPs affects the heat exchanger performance. The FLUENT module of ANSYS version 2020 R1 was used to simulate the flow in a single strip of a crossflow heat exchanger to calculate the heat transfer coefficient and pressure drop. It was performed in low Reynolds number ranges from 550 to 960. Using those RWPs, heat transfer coefficient increases significantly as the converging channel accelerates the local flow around the tube and increases local Reynolds number that also affects in pressure drop also. Forward and backward arrangement provides better performance more specifically the RWPs placed behind the tube provide better performance.

Keywords: Crossflow Heat Exchanger, Rectangular Winglet Pair, Converging Channel, Heat transfer Enhancement.

Copyright @ All authors

This work is licensed under a Creative Commons Attribution 4.0 International License.

## 1. Introduction

Converging channels in cross-flow heat exchangers offer an alternative approach to passive enhancement which is a alternate option of vortex generators like winglets. While vortex generators primarily target the wake region behind tubes to interrupt boundary layer and induce turbulence but in converging channels manipulate the flow path itself. As the channel narrows, the fluid velocity increases as converging channel accelerates the flow, gradually thinning the thermal boundary layer around the tubes and increases turbulence by obtaining the swirling flow with minimal pressure drop.

Biswas et al. [4] numerically analyzed to increase heat transmission utilizing the winglet. This analysis demonstrates that the effect of the winglets placed in cylinder's downstream at the converging region increases heat transmission by up to 240% over the baseline cylinder. Torii et al. [5] experimented in a crossflow heat exchanger to determine heat transfer as well as pressure drop across the heat exchanger with winglet vortex generators in fin-tube crossflow heat exchangers with common upward and downward flow designs. The Reynolds number varied from 250 to 2100. The in-line tube arrangement and staggered tube arrangement of the tube bank suggests heat transfer augmentation in the order of 10-20% and 10-30% respectively, as well as in the pressure drop of 8-15% and 34-55%. Jain et al. [6] and Tiwari et al. [7] extended the work on winglet flow configuration to oval fin-tube cross-flow heat exchangers. By placing delta winglet at backward of the tube surface, they achieved significant separation delay, reduced the wake size, and eliminated the zone of low heat transfer near the tube wake. Their findings reported a 43% improvement in heat transfer for 2 winglet pairs arranged in a staggered tube arrangement. Li et al. [8] investigated the rise in Nu due to increased intensity in secondary flow using numerical simulation on a set of numerous lengthwise vortex generators setups on the fin's flat surface of cylindrical tubes. When more vortex generators are added on the fin surface, the Nu rises by 20% over only fin-tube crossflow heat exchanger. RWPs were also described as it enhance thermal performance as delta vortex generators. The increased converging attack angle of the RWPs improves the thermal performance of the tube bank. Chu et al. [9] investigated the 3D numerical simulation for flow and heat transfer in fin-and-tube heat exchangers using the RWPs. In this case Re varied from 500 to 880, and three arrangements are used: in line with 1RWP case, in line with 3RWP case, and in line with 7RWP case, as well as a baseline cylinder. The results showed that the heat transfer coefficient in the cylinder wall was enhanced up to 43.9%, 87.6%, and 131% for the three enhanced arrangements, with additional pressure penalty increase up to 25.1%, 72%, and 121.4%, respectively. They chose the inline-3RWP case as the optimum because it has a significant minimum pressure drop for maximum heat transfer.

Joardar et al. [10] investigated in an experiment the effect of RWPs arrangement for Single RWP in the 1st tube and 3 RWPs in odd formation in a row of 7 cold tube. The research found that the 3RWPs arrangement as the optimum arrangement. Ya-Ling et al. [11] numerically analyzed heat transfer rate and pressure drop in fin-tube crossflow heat exchangers with RWPs in a 3D geometry. RWPs significantly enhance heat transfer by generating vortices that improve thermal mixing and delay boundary layer separation. The research shows that a single-RWP improves heat transfer by 22.7-25.5% with a 22-24.5% increase in pressure difference, while the 3-RWPs configuration enhances heat transfer by 54.6-61.5% with a 58.1% rise in pressure drop. The 7-RWPs configuration boosts heat transfer by 87.5-105.1% but with a significant pressure drop penalty. Staggered RWP arrays reduce pressure drop by 4.5-8.3% compared to inline arrays. The optimal angle of attack for RWPs is 20° with

*Corresponding Author Email Address: adnan.roshid36@gmail.com 

consideration of maximum heat transfer with minimal pressure drop. Kotcioglu et al. [12] used the entropy generation approach to perform second law analysis and thermal performance in a cross-flow heat exchanger with a rectangular winglet. The results show a 15%-30% increase in heat transfer enhancement and a 20%-30% rise in pressure drop when compared with and without vortex generators. They found that when Re was low, heat transfer dominated entropy generation, whereas at high Reynolds numbers, pressure drop had a greater influence. Jang et al. [13] optimized the span angle of RWPs in fin-tube heat exchanger equipped with rectangular type of block vortex generators. The enhancement was achieved by adjusting the convergence angle from 30° to 60° while maintaining low Re from 400 to 1200. According to the results, the greatest area of surface reduction ratio for inline tube and staggered tube arrangements was 14.9-25.5% and 7.9-13.6%. Wang et al. [14] performed a numerical analysis of a fin-tube crossflow heat exchanger with a RWP and trapezoidal wing for improved heat transmission. The trapezoidal winglet generates a larger vortex than the normal rectangular vortex. In comparison to the RWPs, the Nusselt number as well as pressure drop rise by 2.7-3.8% and 4.7% in trapezoidal winglets. Guan et al. [15] investigated how the geometry of vortex generators affects thermal performance and hydraulic performance of crossflow finned tube banks. Vortex generators came in several shapes, including delta, rectangular, and trapezoidal. Nu number and secondary accelerated flow speed increase as the fluid flow's Reynolds number increases. Delta winglets is found as the most efficient in terms of maximum heat transfer coefficient and minimal pressure decrease. The measurement of the growth in Nu is described in terms of secondary accelerated flow strength at various Re. Delta winglets have a 7-14% higher Nusselt number than RWPs and trapezoidal winglet pairs, also friction factor 17% increased. Salviano et al. [16] numerically analyzed heat transfer performance in staggered and in-line tube arrangement heat exchanger which contains lengthwise vortex generators. For hydraulic performance Colburn and friction factors are employed in optimizing the study for Re 250 to 650. The intensity of the horseshoe vortex was increased with staggered tube system and heat transfer increased by 13% and 26% at Re of 250 and 650, respectively. Mohd et al. [17] investigates the applicability of RWPs to enhance the heat transfer of fin-tube crossflow heat exchangers at low Re. RWPs were placed into two positions: at the span near the tubes and in the span behind the tubes. The results showed that as the angle of RWPs increased, heat transfer generally improved but the drop in pressure increased. Thus, attempts have been made to find an optimal geometry that would give maximum heat transfer with less energy consumption. Dheeraj et al. [18] performed a numerical analysis for non-Newtonian fluid aqueous solution of carboxymethylcellulose in RWP in fin-tube crossflow heat exchanger and found that reducing the angle of attack enhances thermal and hydraulic performance by improving fluid intermixing, but it also causes a notable pressure drop. Heat transfer also increase with Re. Using aqueous carboxymethylcellulose solutions with winglets in the path of the flow also greatly improves the average Nusselt number by 124%-186% and average quality factor by 111%-133% when compared to water.

The objective of this work is to investigate the effect of Converging channel's optimum position in horizontal direction from the center point of tube circle and how it affects heat transfer, Nu and pressure drop. The numerical setup is followed by 2D geometry of previously work done by Joardar et al. [10] experimentally for the winglet arrangement. But they no analysis is available for optimum placement of RWPs from the tube center

## 2. Model description

### 2.1 Geometry

This study looks at a fin-tube crossflow heat exchanger with a longitudinal vortex generator that is utilized in an air-conditioning unit at condenser and evaporator. Also, in car radiator. In **Fig. 1**, the schematic diagram of the heat exchanger is shown. Vortex generators can be classified into four types: delta wings, rectangular wings, delta-winglet pairs, and rectangular winglet pairs. Based on the findings of prior research, we choose the RWP as the converging channel in the current study. RWPs are symmetrically installed on the fin's flat surface, next to the circular tube. The height(H) of the winglets are same as the distance between two adjacent fins. the dimensions and arrangement of rectangular winglets and tubes are shown in **Fig. 2**. RWPs are positioned in a "converging" formation.

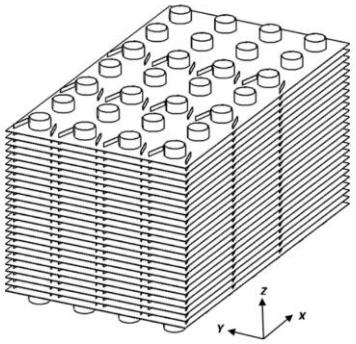


**Fig.1** Schematic diagram a fin-tube cross flow heat exchanger with RWPs core region of [11]

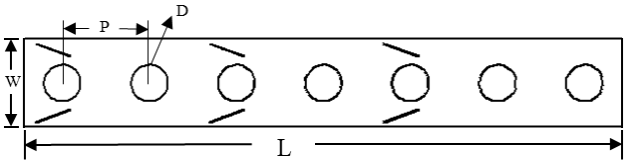


**Fig. 2** Single row of tube and RWPs from the whole surface

From **Fig. 3**, the variable parameter of this geometry is the ratio of vertical and horizontal distance $(\frac{y}{x})$ , the angle of converge, $\alpha = 20°$ with horizontal axis. The vertical distance $y = 7.68mm$ kept constant. The ratio is positive for Forward position and negative for Backward position

### 2.2 Computational Domain

In **Fig. 4** computational domain with coordinate system, with X representing the flow direction and Y representing the spanwise direction is shown. **Fig 3** depicts computational domain from the top for fin-tube crossflow heat exchanger with RWPs. Two nearby fins produce fin to fin distance is same as the RWPs height $H = 3.63\,mm$, width $W = 12.7\,mm$, and length $L = 177.8\,mm$. The dimension first tube's diameter, $D = 10.67\,mm$, is placed at

$l = 12.7\ mm$ from the in late wall. Both the longitudinal and transverse tube pitches are $P = 25.4\ mm$. The length of the RWP is the same as the tube diameter. The tube are arranged in-line. The fin and the RWPs are set as aluminum and the fluid is air. Fin thickness is $F_t = 0.18\ mm$. Because of the high thermal conductivity of the aluminum tube wall, the temperature of the tube is maintained constant. However, the temperature circulation on the fin's flat surface is not determined and it is to be analyzed during the simulation.

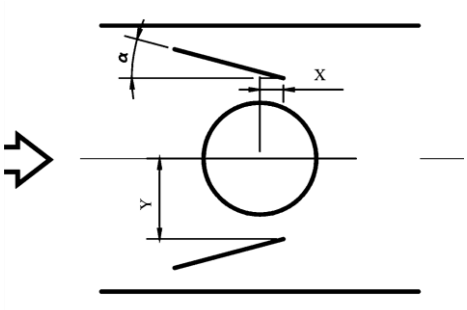


**Fig. 3** Rectangular Winglet Pair (RWP) arrangement with the tube's center

To assure recirculation-free flow and prevent backflow in the outlet, the actual computational domain is extended by 5H at the inlet to maintain uniform velocity, and by 30H at the. The length of the computational domain becomes $L = 304.85\ mm$. Actual computational domain is presented in **Fig.4**.

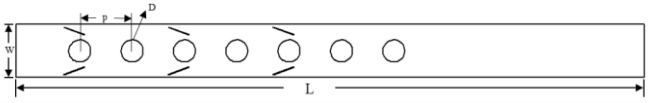


**Fig.4** Computational domain

2.3 Governing equations

The governing equation for any heat transfer system follows Continuity, Momentum and energy equation. Below the equation governing the simulation are mentioned in Cartesian coordinates:

Continuity equation: $\frac{\partial}{\partial x_i}(\rho u_i) = 0$ (1)

Momentum equation: $\frac{\partial}{\partial x_i}(\rho u_i u_k) = \frac{\partial}{\partial x_i}\left(\mu \frac{\partial u_k}{\partial x_i}\right) - \frac{\partial p}{\partial x_k}$ (2)

Energy equation: $\frac{\partial}{\partial x_i}(\rho u_i T) = \frac{\partial}{\partial x_i}\left(\frac{\lambda}{c_p}\frac{\partial T}{\partial x_i}\right)$ (3)

2.4 Boundary Condition

The boundary condition is defined as the Symmetry condition in upper and lower surface due to the computational domain is cut from a surface with symmetric strip of tubes and RWPs. Inlet in the left side is a velocity inlet with temperature 310.6 K and the tube walls are wall with temperature 291.77 K. Velocity at inlet varies from 1.18 m/s to 2.05 m/s for the respected Re ranges from 550 to 960.

2.4 Parameter definitions

The Reynolds number (Re), average Nusselt number (Nu) are defined as follows:

$$\mathrm{Re} = \rho V_m D_h/\mu, \qquad Nu = hD_h/\lambda \tag{4}$$

The average temperature and pressure at an arbitrary wall can be found from the equations below:

$$\bar{T} = \frac{\iint_A uTdA}{\iint_A udA}, \qquad \bar{p} = \frac{\iint_A pdA}{\iint_A dA} \tag{5}$$

Total heat transfer: $Q = \dot{m}c_p(\bar{T}_{out} - \bar{T}_{in})$ (6)

Pressure loss: $\Delta P = \bar{p}_{in} - \bar{p}_{out}$ (7)

Log Mean Temperature Difference (LMTD):

$$\Delta T = \frac{(T_w - \bar{T}_{in}) - (T_w - \bar{T}_{out})}{In[(T_w - \bar{T}_{in})/(T_w - \bar{T}_{out})]} \tag{8}$$

Heat transfer coefficient: $h = \frac{Q}{A_T \Delta T} = \frac{q}{\Delta T}$ (9)

2.5 Numerical Method

The 2D geometry is sketched in SolidWorks Drawing and imported it to ANSYS 2020 for generating mesh. As the flow is laminar due to low Re number the meshing was performed unstructured and triangular mesh for the whole region. **Fig. 5** shows the meshing performed. The governing equations and boundary conditions are solved using CFD models (ANSYS Fluent 2020). The second-order upwind technique is used to separate the convective terms found in the governing equations. Additionally, the SIMPLE algorithm is employed to obtain the velocity, temperature and pressure fields. The convergence criterion for the continuity, momentum, and energy equations are $10^{-3}$, $10^{-3}$, and $10^{-6}$, respectively. The governing equations were solved with iteration till the corresponding residual values were attained or stabilized at constant values. [19]

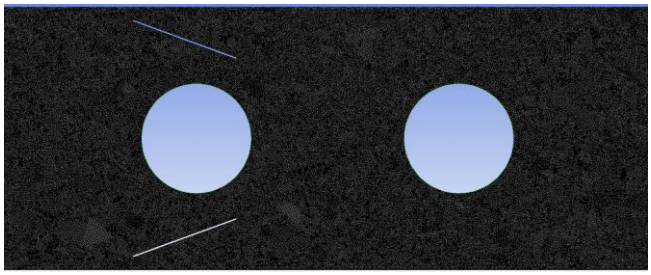

**Fig. 5** Mesh around Tube and RWPs

2.6 Mesh Independence Test

To prove mesh independence, a range of grid solutions are studied, including about 19552, 58590, 948310, and 3728855 cells for the fined-tube crossflow heat exchanger with three RWPs. **Fig. 6** depicts the expected averaged Nu numbers achieved in four grid systems with different element number. From the graph it is analyzed that the averaged Nu number varies. For, first 3 grid system there are a big difference between them. But there is 0.145% difference between 948310 and 3728855 cells. For this

simulation element number is selected as about 948310 instead of 3728855 to save computational process.

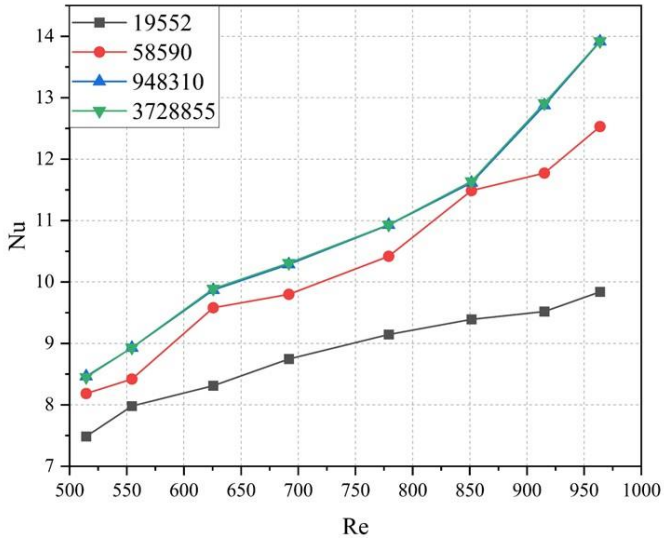


**Fig.6** Predicted Nusselt number versus different elements number.

## 3. Validation

The computational results were validated by comparing heat transfer coefficient to the existing experimental results. To check the dependability of the numerical method, a numerical simulation of a fin-tube crossflow heat exchanger with 3RWPs is performed, as described in Joardar et al. [12]. The input air velocity varies from 1.18 to 2.05 m/s, with respected Re numbers ranging from 550 to 960.

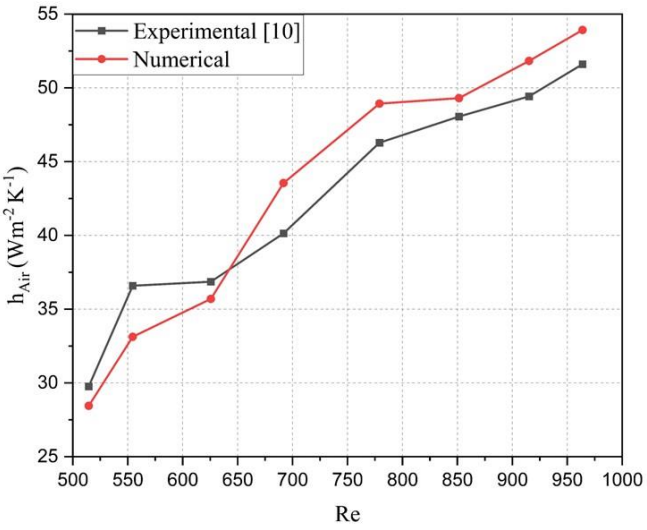


**Fig.6** Experimental and Numerical comparison of $h_{Air}$ for validation in different Re

The average difference between experimental [10] and numerical heat transfer coefficients is 5.41% which is considearble. Because the contact resistance and leaking of the experimental setup were unavoidable. However, the numerical simulation comes near to perfect conditions. The closeness of the results between projected and experimental results demonstrates that the current numerical method is trustworthy to forecast thermal parameters and flow characteristics in crossflow heat exchanger.

## 4. Results and discussions

The average heat flux from the tube wall is calculated from the solution and then the average outlet temperature from the outlet is used for calculating heat transfer coefficient and the static pressure difference at inlet and outlet provides the pressure drop.

### 4.1 Forward Arrangement

When the RWPs are placed ahead of the tube center then the heat transfer coefficient is increasing from baseline arrangement. The more the ratio increases the closer the RWPs around the tube. Form **Fig. 7,** the maximum heat transfer coefficient achieved from ratio 4. And the pressure penalty is considerably high but less than ratio 3 arrangement in **Fig. 8.** It is because the converging accelerates the local air to increase velocity also Re shown in **Fig. 11**.

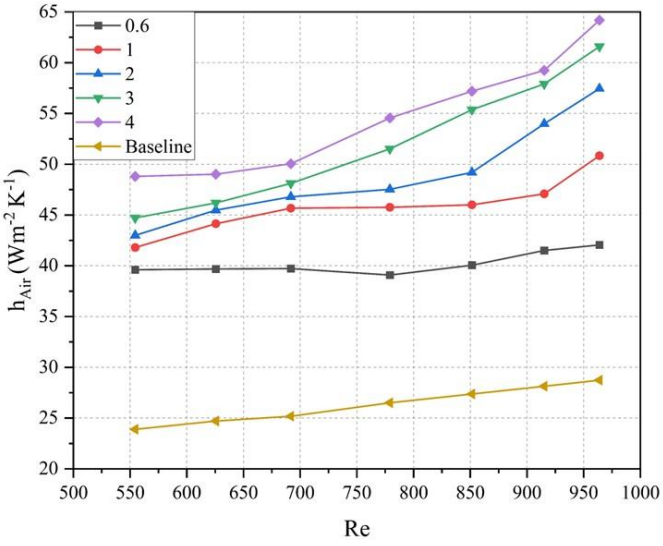


**Fig.7** Enhancement of the $h_{Air}$ at tube wall vs the $Re$ number for Forward arrangement.

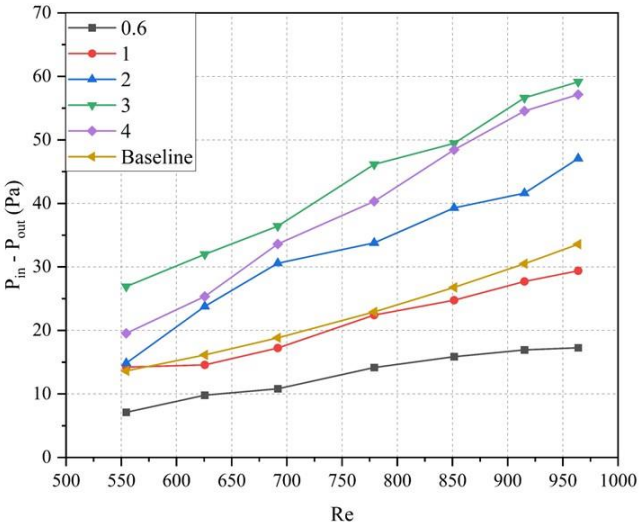


**Fig.8** Enhancement of Pressure loss ($P_{in} - P_{out}$) vs the $Re$ number for Forward arrangement.

For the RWP position in the forward middle with ratio 0.604 the pressure drop is reduced as the effect of converging channel is not sufficient to reach the tube wall that helps heat transfer enhancement. The temperature distribution is irregular due to low Re shown in **Fig.12.**

Although, the ratio 4 arrangement shows 98% average increase in heat transfer coefficient than baseline arrangement with no RWP.

4.2 Backward Arrangement

When the RWPs are placed in behind the tube center then the heat transfer coefficient is increasing and decreasing from baseline arrangement. The more the ratio increases the closer the RWPs around the tube. Form **Fig. 9,** the maximum heat transfer coefficient achieved from ratio -2. And the pressure penalty is considerably high but less than ratio -3 and ratio -4 arrangement in **Fig. 10.** It is because the converging accelerates the local air to increase velocity also Re shown in **Fig. 11.** For the RWP position in the backward middle with ratio -0.604 and ratio -1 the heat transfer is reduced as the effect of converging channel is not sufficient to reach the tube wall that helps heat transfer enhancement. The temperature distribution is irregular due to low Re shown in **Fig.12.** Although, the ratio -2 arrangement shows 103% average increase than baseline arrangement with no RWP.

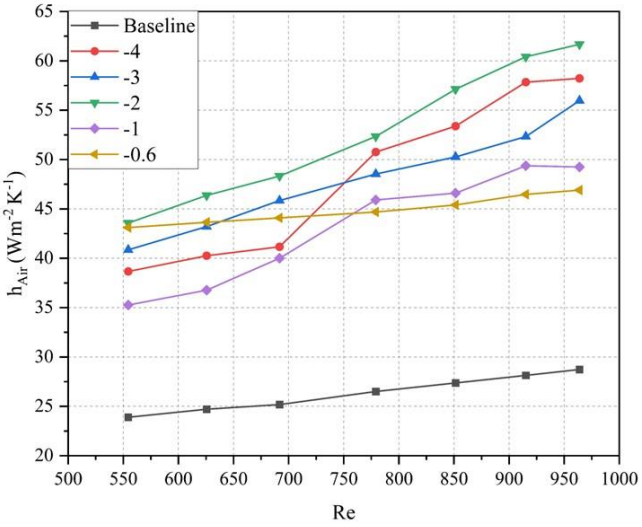


**Fig.9** Enhancement of the $h_{Air}$ at tube wall vs the $Re$ number for Backward arrangement.

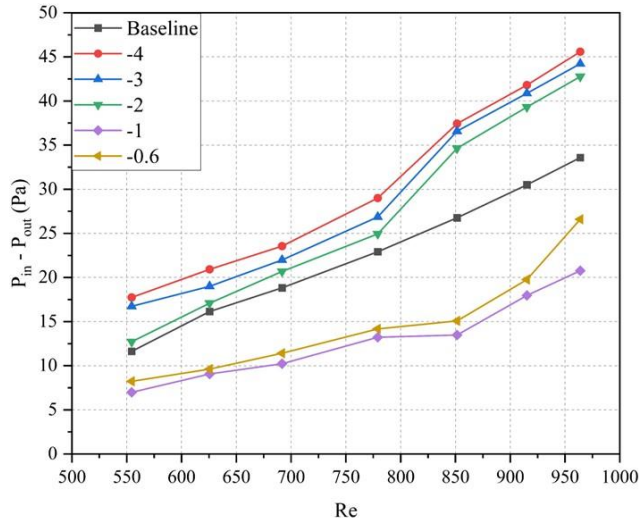


**Fig.10** Enhancement of Pressure loss $(P_{in} - P_{out})$ vs the $Re$ number for Backward arrangement.

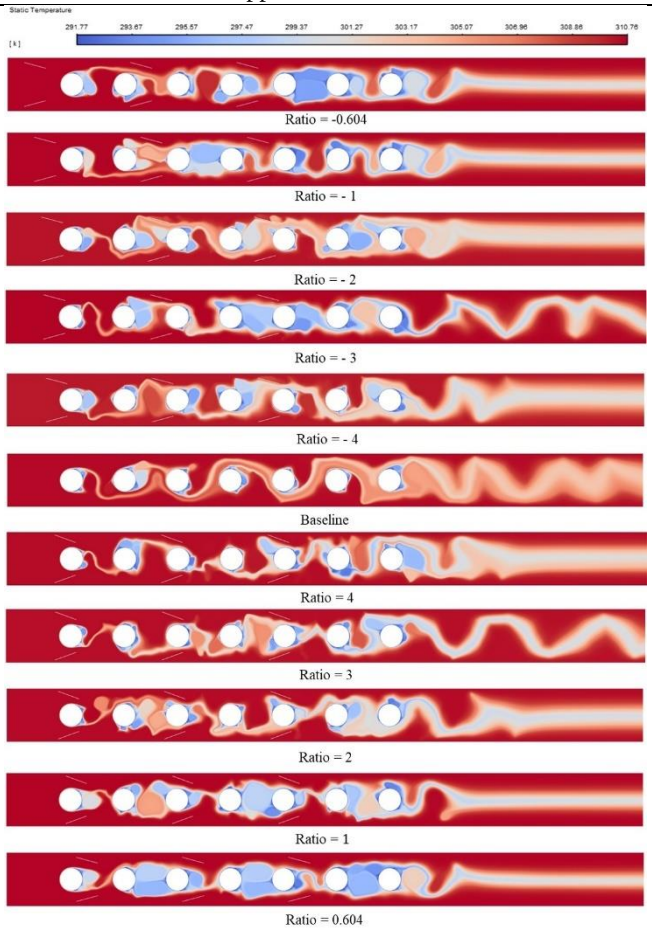


**Fig.11** Temperature Contour for different RWP position.

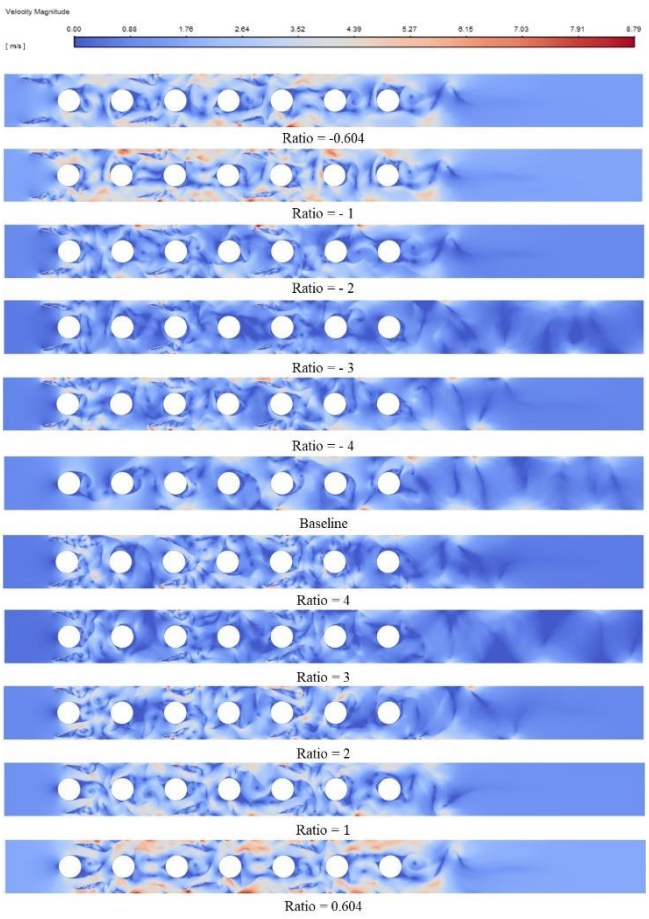


**Fig.12** Velocity Contour for different RWP position

## 5. Conclusion

In this paper the effect of converging channel in crossflow heat exchanger is investigated. The forward and backward arrangement both provide enhancement in heat transfer performance about 98-103% than tubes with no RWPs. But the backward arrangement with ratio -2 provide improved heat transfer coefficient up to 5% than forward arrangement ratio 4 with minimal pressure drop due to converging effect in the flow. In this study vertical distance kept constant and the horizontal distance is varied. For future scope is to optimize both distance for optimum heat transfer coefficient and pressure drop.

## References


[1] Mangrulkar, C. K., Dhoble, A. S., Chamoli, S., Gupta, A., & Gawande, V. B. (2019). Recent advancement in heat transfer and fluid flow characteristics in cross flow heat exchangers. Renewable and Sustainable Energy Reviews, 113, 109220.

[2] Bejan, A. (2013). Convection heat transfer. John wiley & sons.

[3] Liang, G., Islam, M. D., Kharoua, N., & Simmons, R. (2018). Numerical study of heat transfer and flow behavior in a circular tube fitted with varying arrays of winglet vortex generators. International Journal of Thermal Sciences, 134, 54-65.

[4] Biswas, G., Mitra, N. K., & Fiebig, M. (1994). Heat transfer enhancement in fin-tube heat exchangers by winglet type vortex generators. *International Journal of Heat and Mass Transfer*, *37*(2), 283-291.

[5] Torii, K., Kwak, K. M., & Nishino, K. (2002). Heat transfer enhancement accompanying pressure-loss reduction with winglet-type vortex generators for fin-tube heat exchangers. *International Journal of Heat and Mass Transfer*, *45*(18), 3795-3801.

[6] Jain, A., Biswas, G., & Maurya, D. (2003). Winglet-type vortex generators with common-flow-up configuration for fin-tube heat exchangers. Numerical Heat Transfer: Part A: Applications, 43(2), 201-219.

[7] Tiwari, S., Maurya, D., Biswas, G., & Eswaran, V. (2003). Heat transfer enhancement in cross-flow heat exchangers using oval tubes and multiple delta winglets. International Journal of Heat and Mass Transfer, 46(15), 2841-2856.

[8] Li, L., Du, X., Zhang, Y., Yang, L., & Yang, Y. (2015). Numerical simulation on flow and heat transfer of fin-and-tube heat exchanger with longitudinal vortex generators. International Journal of Thermal Sciences, 92, 85-96.

[9] Chu, P., He, Y. L., & Tao, W. Q. (2009). Three-dimensional numerical study of flow and heat transfer enhancement using vortex generators in fin-and-tube heat exchangers.

[10] Joardar, A., & Jacobi, A. M. (2008). Heat transfer enhancement by winglet-type vortex generator arrays in compact plain-fin-and-tube heat exchangers. *International journal of refrigeration*, *31*(1), 87-97.

[11] He, Y. L., Chu, P., Tao, W. Q., Zhang, Y. W., & Xie, T. (2013). Analysis of heat transfer and pressure drop for fin-and-tube heat exchangers with rectangular winglet-type vortex generators. Applied Thermal Engineering, 61(2), 770-783.

[12] Kotcioglu, I., Caliskan, S., Cansiz, A., & Baskaya, S. (2010). Second law analysis and heat transfer in a cross-flow heat exchanger with a new winglet-type vortex generator. Energy, 35(9), 3686-3695.

[13] Jang, J. Y., Hsu, L. F., & Leu, J. S. (2013). Optimization of the span angle and location of vortex generators in a plate-fin and tube heat exchanger. International Journal of Heat and Mass Transfer, 67, 432-444.

[14] Wang, W., Bao, Y., & Wang, Y. (2015). Numerical investigation of a finned-tube heat exchanger with novel longitudinal vortex generators. Applied Thermal Engineering, 86, 27-34.

[15] Hu, W., Wang, L., Guan, Y., & Hu, W. (2017). The effect of shape of winglet vortex generator on the thermal–hydrodynamic performance of a circular tube bank fin heat exchanger. Heat and Mass Transfer, 53, 2961-2973.

[16] Salviano, L. O., Dezan, D. J., & Yanagihara, J. I. (2016). Thermal-hydraulic performance optimization of inline and staggered fin-tube compact heat exchangers applying longitudinal vortex generators. Applied Thermal Engineering, 95, 311-329.

[17] Zeeshan, M., Nath, S., Bhanja, D., & Das, A. (2018). Numerical investigation for the optimal placements of rectangular vortex generators for improved thermal performance of fin-and-tube heat exchangers. *Applied Thermal Engineering*, *136*, 589-601.

[18] Kumar, D., & Dalal, A. (2024). A numerical study of the thermal and hydraulic parameters of a finned tube heat exchanger using shear-thinning fluid and rectangular winglet. *International Journal of Thermal Sciences*, *195*, 108653.

[19] Zeeshan, M., Nath, S., & Bhanja, D. (2017). Numerical study to predict optimal configuration of fin and tube compact heat exchanger with various tube shapes and spatial arrangements. *Energy Conversion and Management*, *148*, 737-752.


## NOMENCLATURE

$\rho$ : density, $m^3$
$A$ : Area, $m^2$
$\dot{m}$ : mass flow rate, kg/s
$c_p$ : specific heat at constant pressure, $kJ \cdot kg^{-1} \cdot K^{-1}$
$\bar{T}$ : mean temperature, K
$\bar{p}$ : mean pressure, Pa
$T_w$ : wall temperature, K
$A_T$ : Tube wall area, $m^2$
$h$ : convective Heat Transfer coefficient, $W/m^2$
$V_m$ : average velocity at the minimum cross-section of the flow channel
$\mu$ : dynamic viscosity of fluid
$\lambda$ : thermal conductivity
$D_h$ : hydraulic diameter